



UNIVERSITY OF LEEDS

This is a repository copy of *Enhanced-Range Intrusion Detection Using Pyroelectric Infrared Sensors*.

White Rose Research Online URL for this paper:
<http://eprints.whiterose.ac.uk/104689/>

Version: Accepted Version

Proceedings Paper:

Aldalahmeh, SA, Hamden, AM, Ghogho, M orcid.org/0000-0002-0055-7867 et al. (1 more author) (2016) *Enhanced-Range Intrusion Detection Using Pyroelectric Infrared Sensors*. In: *Sensor Signal Processing for Defence (SSPD)*, 2016. *Sensor Signal Processing for Defence Conference*, 22-23 Sep 2016, Edinburgh, Scotland. IEEE . ISBN 978-1-5090-0326-6

<https://doi.org/10.1109/SSPD.2016.7590597>

© 2016, IEEE. Personal use of this material is permitted. Permission from IEEE must be obtained for all other users, including reprinting/ republishing this material for advertising or promotional purposes, creating new collective works for resale or redistribution to servers or lists, or reuse of any copyrighted components of this work in other works.

Reuse

Unless indicated otherwise, fulltext items are protected by copyright with all rights reserved. The copyright exception in section 29 of the Copyright, Designs and Patents Act 1988 allows the making of a single copy solely for the purpose of non-commercial research or private study within the limits of fair dealing. The publisher or other rights-holder may allow further reproduction and re-use of this version - refer to the White Rose Research Online record for this item. Where records identify the publisher as the copyright holder, users can verify any specific terms of use on the publisher's website.

Takedown

If you consider content in White Rose Research Online to be in breach of UK law, please notify us by emailing eprints@whiterose.ac.uk including the URL of the record and the reason for the withdrawal request.



eprints@whiterose.ac.uk
<https://eprints.whiterose.ac.uk/>

Enhanced-Range Intrusion Detection Using Pyroelectric Infrared Sensors

Sami A. Aldalahmeh^{1,†}, Amer M. Hamdan^{1,†}, Mounir Ghogho^{2,3,‡} and Des McLernon^{2,‡}

¹ Al-Zaytoonah University of Jordan, Jordan, ² Leeds University, UK.

³ International University of Rabbat, Morocco.

[†] {s.aldalahmeh, a.hamdan}@zuj.edu.jo, [‡] {m.ghogho, d.c.mclernon}@leeds.ac.uk.

Abstract—In this paper, the problem of intrusion detection using passive infrared sensors (PIR) is investigated. We study the output PIR signal in the light of the intruder’s trajectory and the geometry of the sensor’s field of view (FOV) and propose an inverse-square law that describes the relation of incident heat flux to the distance. The signal is modeled by a sum of exponentially modulated sinusoids. Consequently, the intrusion detection is formulated as a hypothesis testing problem and we propose an exponentially windowed periodogram (EWP) detector, which is also able to detect the direction of movement. The simulation results shows the superior performance of the EWP detector when compared to conventional detectors such as the traditional periodogram detector and the energy detector over large distances. Furthermore, results show nearly 100% correct detection of the direction of movement.

I. INTRODUCTION

Intrusion detection is a vital field of research with significant practical impact. Several sensor modalities are used for intrusion detection, some of which are magnetic, acoustic, seismic, and thermal sensors [1]. However, pyroelectric infrared (PIR) sensors present themselves as an attractive option due to their low power requirement, low cost, and small form factor. PIR sensors are made from pyroelectric crystals that are intrinsically polarized [2]. When exposed to temperature change, the polarization is temporally disturbed producing a current proportional to the heat gradient. Thus, PIR sensors measure the change in temperature making them suitable for motion detection. Usually, two sensor elements are connected serially in reverse polarity, thus producing a positive voltage when motion occurs in the positive element field of view (FOV) and a negative voltage when motion occurs in the negative element’s FOV. Hence, PIR sensors can be found in many indoor applications, such as [3]. Recently, PIR sensors were also used with wireless sensor networks (WSNs) in outdoor applications [4], due to the previously stated features. However, due to limited detection range the outdoor applications are limited. Therefore, advanced processing techniques are needed in order to increase the detection range of the PIR sensors

Several processing methods have been suggested in the literature. In [5], energy detection with adaptive noise threshold was proposed. Simple high-pass filtering was also used to improve the SNR. A combination of the Haar transform and support-vector-machine was used in [6] to detect intrusion in the presence of clutter. In [7], the authors proposed using a linear regression model in conjunction with hidden Markov

models to detect and classify human walking movement. PIR sensors were used for tracking of direction and distance of motion in [8] via feature extraction methods. A set of two orthogonal PIR sensor pairs were used in [9] to detect the direction of movement.

In this paper we investigate increasing the detection range of PIR in outdoor environments using the statistical hypothesis testing framework leading to advanced signal processing methods, in contrast to the simplified processing adopted in [6]. Firstly, we show that the incident heat flux at the sensor obeys the inverse square law for an arbitrary source shape. Secondly, we model the incident heat flux time varying signal as a function of the intruders’ trajectory parameters. Finally, we formulate the detection problem as multiple hypothesis testing.

This paper is organized as the following. Section II presents the system model. In Section III, the detection problem is formulated and the corresponding detection algorithms are proposed. Simulation results are provided in IV. Finally, the conclusions and future work are given in Section V.

II. MODELING OF INTRUDER’S SIGNATURE

In this section the time-varying heat flux signature generated by the intruder and the PIR sensor are formulated.

A. Intruder Heat Flux

We are interested in measuring the heat flux generated by a mobile intruder moving with constant speed and direction. The intruder is assumed to be in thermal equilibrium with its environment. The measured flux at the sensor mainly depends on the temperature, source geometry, and the spatial orientation of the intruder and the sensor with respect to (wrt) each other. Assuming a Lambertian grey body emitting uniformly in space, the heat flux at the sensor is [2]

$$\Phi = \frac{1}{\pi} \varepsilon k_B \omega_{i,s} (T_i^4 - T_e^4) A_i \quad (1)$$

where $0 < \varepsilon < 1$ is the intruder’s emissivity, $k_B \approx 1.381 \times 10^{-23} \text{kg.m}^2/\text{s}^2\text{K}$ is the Steveman-Boltzmann constant, T_i is the intruder’s absolute temperature, T_e is the environment’s temperature, A_i is the intruder’s surface area, and $\omega_{i,s}$ is the projected solid angle of the intruder onto the sensor. So the geometry of the source w.r.t. the sensor is given by

$$\omega_{i,s} = \frac{1}{A_s} \int_{A_i} \int_{A_s} \frac{\cos \beta_i \cos \beta_s}{R_{i,s}^2} dA_i dA_s \quad (2)$$

where A_s is the sensor’s area, β_i and β_s are the angles of dA_i and dA_s wrt to the axis connecting them, and $R_{i,s}$ is the

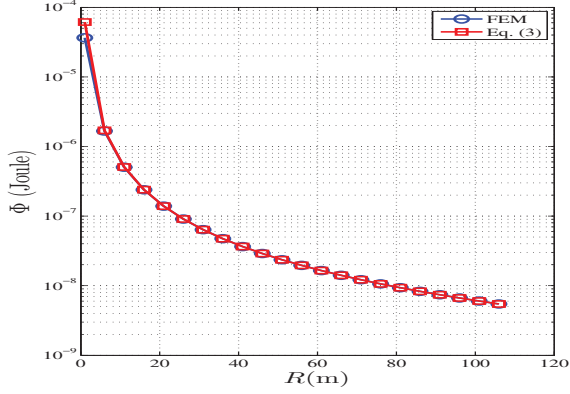


Fig. 1: Heat flux, Φ , as a function of distance R for the FEM and the approximation in (3). The human source is modeled by a rectangular head and body with dimensions of $0.22\text{m} \times 0.14\text{m}$ and $1.7\text{m} \times 0.4\text{m}$ respectively. The human temperature is $T_i = 37^\circ$ with emissivity $\varepsilon = 1$, environment temperature $T_e = 20^\circ$, sensor area $A_s = 20\mu\text{m}^2$, intruder area $A_i = 0.7\text{m}^2$.

distance separating the infinitesimal elements dA_i and dA_s . Consequently, the total heat flux is found by solving the double integration in (1) and substituting in (1).

For an arbitrary geometry, the incident heat flux is usually found by the finite element method (FEM), which is known to be cumbersome. Instead, we propose the following closed-form approximation

$$\Phi \approx \varepsilon k_B (T_i^4 - T_e^4) \frac{A_i A_s}{4R^2}. \quad (3)$$

which is simply an inverse square law relationship. The above approximation is compared with the FEM results in (1) for a human source at different distances. The results show excellent matching with our approximation for distances greater than 5 meters.

As the intruder passes in front of the PIR sensor, a Fresnel lens modulates the incident heat flux by partitioning the FOV into multiple segments¹ as shown in Fig. 2(a), where each segment concentrates the flux onto the PIR sensor. Consequently, the PIR sensor's signal depends on the intruder's trajectory through the FOVs. Take for example an intruder crossing the central FOV segment with constant speed v making an angle ψ_0 with the main sensor axis at distance R_0 as shown in Fig. 2(b). The squared distance between the intruder and the sensor is given by the cosine rule [6] as

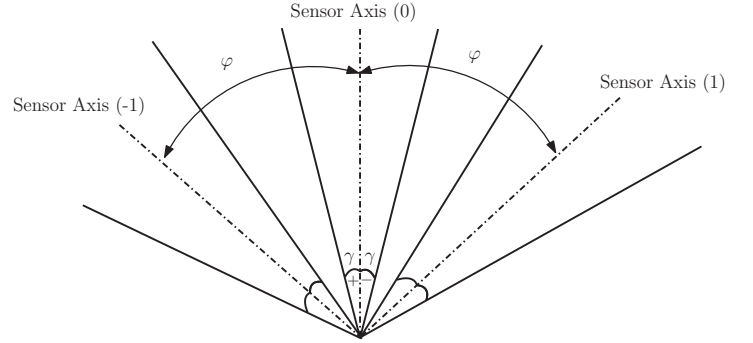
$$R^2(t) = v^2 t^2 + \left(\frac{R_0 \sin \psi_0}{\sin(\psi_0 + \gamma)} \right)^2 + \frac{2vtR_0 \sin \psi_0}{\tan(\psi_0 + \gamma)}. \quad (4)$$

Therefore, the incident heat flux has the form

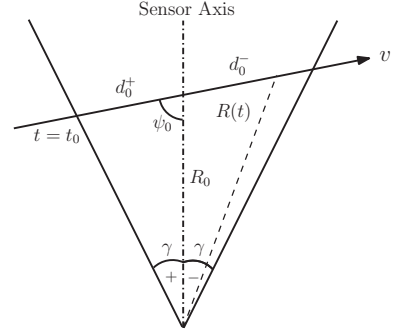
$$\Phi(t) = \frac{\tilde{\Phi}}{R^2(t)} \left[\Pi \left(\frac{t - t_0}{d_0^+ / v} \right) - \Pi \left(\frac{t - t_0 - d_0^+ / v}{d_0^- / v} \right) \right] \quad (5)$$

where $\tilde{\Phi} = \varepsilon k_B (T_i^4 - T_e^4) A_i A_s / 4$, t_0 is the entry time, and $\Pi(t)$ is a unit rectangular function in the time interval

¹In the context of intrusion detection, such an arrangement increases the probability of detection.



(a) Multiple-segment FOV Fresnel lens configuration. Each segment has a FOV with angle 2γ .



(b) Intruder crossing FOV.

Fig. 2: Intruder crossing the FOV of the Fresnel lens.

$[0, 1]$. In general, For $(2F + 1)$ FOV segments indexed by $j = -F, \dots, F$, we have $\psi_j = \psi_0 - j\varphi$ for $j \neq 0$. Thus, the heat flux signature has the form

$$\Phi(t) = \frac{\Phi_0}{R^2(t)} \sum_{i=-F}^F \left[\Pi \left(\frac{t - t_j}{d_j^+ / v} \right) - \Pi \left(\frac{t - t_j - d_j^+ / v}{d_j^- / v} \right) \right] \quad (6)$$

where t_j is the j th segment entry time.

Figs. 3(a) and 3(b) show the heat flux signal for an intruder moving toward and away from the sensor.

B. PIR Signal

The PIR sensor converts the impinging heat flux into an electrical voltage. The responsivity, which is the ratio of the output voltage to the input heat flux, completely characterizes the sensor. The responsivity is actually a bandpass system [10] given by

$$H(s) = \frac{V(s)}{\Phi(s)} = \frac{Ks}{(1 + \tau_t s)(1 + \tau_e s)} \quad (7)$$

where K is the sensor's gain, τ_t is the thermal time constant of the sensor, and τ_e is the electrical time constant. Therefore, the output voltage signal is a filtered version of the heat flux in (6), i.e.,

$$\begin{aligned} s(t) &= h(t) * \Phi(t) \\ &= \frac{\Phi_0}{R^2(t)} \sum_{i=0}^{F-1} h(t) * \Pi \left(\frac{t - t_i}{d_i / v} \right) \end{aligned} \quad (8)$$

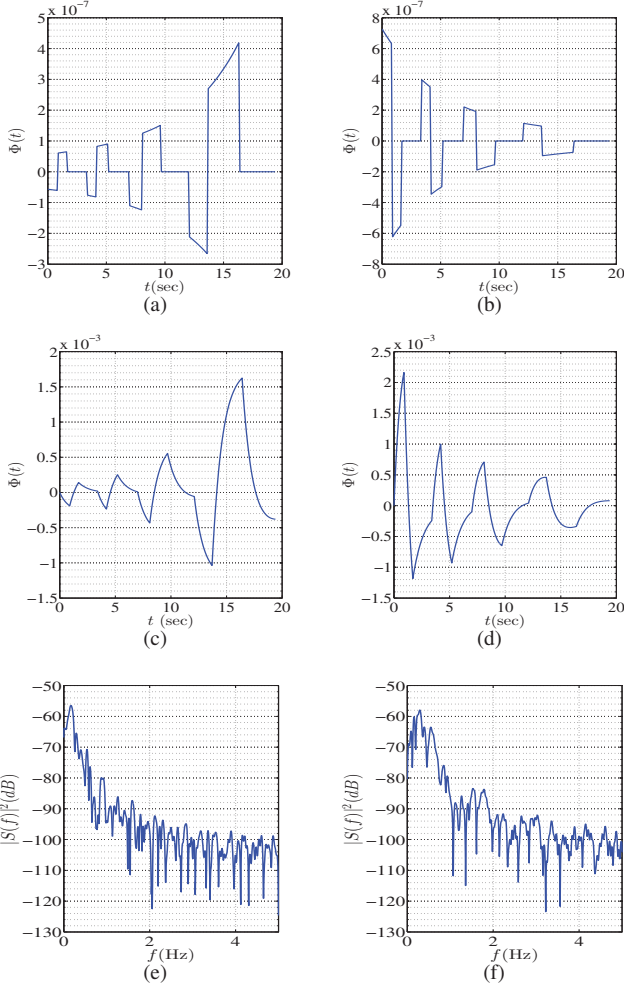


Fig. 3: For an intruder with $R_0 = 50\text{m}$, $v = 5\text{ kmph}$, and $\psi = 50^\circ$, Figs. (a) and (b) show the heat flux, Figs (c) and (d) show the sensor signal for $K = 6 \times 10^3$, $\tau_T = 4.2\text{ sec}$, and $\tau_E = 1\text{ sec}$. Figs. (e) and (f) show the periodograms of the sensor signal sampled with $F_s = 10\text{ Hz}$ and a FFT length of 2048. The first column is for the intruder moving toward the sensor and the second column for it moving away.

where $h(t)$ is the sensor's time-domain responsivity and $*$ is the convolution operator. An example is given in Figs. 3(c) and 3(d).

The PIR sensor elements are usually followed by a JFET voltage buffer, which superimposes the sensor signal on a dc bias of the transistor. Also, the signal is corrupted by noise, which is dependent on the sensor and the environment background heat radiation. However, we assume that the voltage signal at the input of the analog to digital converter, $x(t)$, is appropriately conditioned to remove the dc bias and reduce the noise before being sampled at a sampling frequency of F_s . Hence, the raw available sensor is

$$x[n] = s[n] + w[n]$$

for $0 \leq n \leq N-1$ where $w[n]$ is assumed to be additive white Gaussian noise with zero mean and known variance, σ^2 .

III. INTRUSION DETECTION

For a given intruder's class (e.g. humans) the signal's energy is dependent on the separation distance, since the intruder's energy and the sensor's noise energy are fixed. Hence, we resort to statistical hypothesis testing methods to provide acceptable performance. The intrusion detection problem is formulated as the following hypothesis testing problem, i.e.,

$$\begin{aligned} \mathcal{H}_0 : x[n] &= w[n], & 0 \leq n \leq N-1 \\ \mathcal{H}_1 : x[n] &= s[n] + w[n], & 0 \leq n \leq N-1. \end{aligned} \quad (9)$$

One way to tackle this problem is to assume that $s[n]$ is completely unknown, and so the optimal detector in this case would be the energy detector (ED), with the following test statistics

$$T_{\text{ED}}(\mathbf{x}) = \frac{1}{\sigma^2} \sum_{n=0}^{N-1} x^2[n]. \quad (10)$$

Unfortunately, the energy detector has the worse performance among all detectors, since no prior information is used.

Interestingly, we can infer some valuable information from the shape of the PIR signal. Indeed, $s(t)$ in Fig 3(c) has a striking resemblance to an exponentially decaying sinusoid and to an exponentially increasing sinusoid in Fig. 3(d). This observation is also consolidated by (8). Furthermore, Figs 3(e) and 3(f) suggest having several dominant sinusoidal components. Hence, we propose the following approximation

$$\begin{aligned} s[n] &\approx \sum_{i=0}^{L-1} \alpha^n A_i \cos(2\pi f_i n + \phi_i) \\ &= \sum_{i=0}^{L-1} a_i \alpha^n \cos(2\pi f_i n) + b_i \alpha^n \sin(2\pi f_i n) \end{aligned} \quad (11)$$

where A_i, f_i, ϕ_i are the i th amplitude, frequency, and phase of the i th component respectively. Whereas $\alpha \geq 0$ is the exponential factor and the parameter vector, $a_i = A_i \cos(\phi_i)$ and $b_i = A_i \sin(\phi_i)$. The above can be compactly represented in vector format as

$$\mathbf{s} = \mathbf{G}(\boldsymbol{\theta})\mathbf{c} \quad (12)$$

$$\mathbf{c} = (a_0, \dots, a_{L-1}, b_0, \dots, b_{L-1})^T \quad (13)$$

$$\mathbf{G}(\boldsymbol{\theta}) = \begin{pmatrix} \mathbf{g}_c(\alpha, f_0) \cdots \mathbf{g}_c(\alpha, f_{L-1}) & \mathbf{g}_s(\alpha, f_0) \cdots \mathbf{g}_s(\alpha, f_{L-1}) \end{pmatrix} \quad (14)$$

where $\mathbf{s} = (s[0], \dots, s[N-1])^T$, the signal parameters are lumped in $\boldsymbol{\theta} = (\alpha, f_0, \dots, f_{L-1})^T$, and the columns of the matrix $\mathbf{G}(\boldsymbol{\theta})$ are

$$\mathbf{g}_c(\alpha, f_i) = \left(1, \alpha \cos(2\pi f_i), \dots, \alpha^{N-1} \cos(2\pi f_i(N-1))\right)^T \quad (15)$$

$$\mathbf{g}_s(\alpha, f_i) = \left(0, \alpha \sin(2\pi f_i), \dots, \alpha^{N-1} \sin(2\pi f_i(N-1))\right)^T \quad (16)$$

Consequently, the detection problem can be formulated as

$$\begin{aligned} \mathcal{H}_0 : \mathbf{x} &= \mathbf{w} \\ \mathcal{H}_1 : \mathbf{x} &= \mathbf{G}(\boldsymbol{\theta})\mathbf{c} + \mathbf{w} \end{aligned} \quad (17)$$

where $\mathbf{x} = (x[0], x[1], \dots, x[N-1])^T$ and $\mathbf{w} = (w[0], w[1], \dots, w[N-1])^T$. The above is a composite hypothesis testing, since $\boldsymbol{\theta}$ needs to be estimated. An asymptotically optimal detector is the generalized likelihood ratio test (GLRT) [11]. It can be shown that the GLRT reduces to finding the best projection of \mathbf{x} onto the space spanned by the columns of $\mathbf{G}(\boldsymbol{\theta})$, i.e.,

$$T_{\text{GLRT}}(\mathbf{x}) = \max_{\boldsymbol{\theta}} \|P_{\mathbf{G}}(\boldsymbol{\theta})\mathbf{x}\|^2 \quad (18)$$

where $P_{\mathbf{G}}(\boldsymbol{\theta}) = (\mathbf{G}^T(\boldsymbol{\theta})\mathbf{G}(\boldsymbol{\theta}))^{-1} \mathbf{G}(\boldsymbol{\theta})^T$ is the projection matrix on the space spanned by the columns of $\mathbf{G}(\boldsymbol{\theta})$.

Apparently, the GLRT is computationally demanding mainly due to the non-zero correlation between the columns of $\mathbf{G}(\boldsymbol{\theta})$. Consequently, we propose a sub-optimal detector in which we assume orthogonal columns in $\mathbf{G}(\boldsymbol{\theta})$. In other words,

$$\sum_{i=0}^{L-1} \sum_{j=0}^{L-1} \mathbf{g}_c^T(\alpha, f_i) \mathbf{g}_s(\alpha, f_j) = \begin{cases} N, & i = j \\ 0, & i \neq j \end{cases} \quad (19)$$

for all α and f_i 's. Hence, the resulting detector in this case has the form

$$T(\mathbf{x}) = \max_{\alpha, f_0, \dots, f_{L-1}} \frac{1}{N} \sum_{i=0}^{L-1} |\mathbf{x}^T \mathbf{g}_c(\alpha, f_i)|^2 + |\mathbf{x}^T \mathbf{g}_s(\alpha, f_i)|^2 \quad (20)$$

which for a given α is a separable maximization problem, i.e., it has L peaks at the optimal frequencies (\hat{f}_i) values.

The detector in (20) can be further simplified by noting that the correlations $\mathbf{x}^T \mathbf{g}_c(\alpha, f_i)$ and $\mathbf{x}^T \mathbf{g}_s(\alpha, f_i)$ can be decomposed into two steps. First, multiply the data samples, $x[n]$, by the *window* function α^n for a given α and $0 \leq n \leq N-1$. Defined the windowed data $x_\alpha[n]$ and then the detector in (20) becomes

$$T_{\text{EWP}}(\mathbf{x}) = \max_{\alpha, f_0, \dots, f_{L-1}} \frac{1}{N} \sum_{i=0}^{L-1} |X_\alpha(f_i)|^2 \quad (21)$$

which we will call the exponentially windowed periodogram (EWP) detector. $X_\alpha(f_i)$ in (21) is the windowed periodogram defined as

$$X_\alpha(f_i) = \sum_{n=0}^{N-1} x_\alpha[n] e^{-j2\pi f_i n}. \quad (22)$$

Thus, the EWP detector chooses the window that gives the greatest L spectral peaks. It follows that the periodogram detector (PD) is a special case of the EWP detector when α is fixed at unity, giving

$$T_P(\mathbf{x}) = \max_{f_0, \dots, f_{L-1}} \sum_{i=0}^{L-1} |X_1(f_i)|^2. \quad (23)$$

Interestingly, the optimal window, $\hat{\alpha}$, found earlier gives an indication about the movement direction. If $\hat{\alpha} < 1$ then the signal is decreasing with time implying that the intruder

is moving away from the sensor. Oppositely, if $\hat{\alpha} > 1$ the intruder is moving toward the sensor. Thus,

Decide intruder is moving away from sensor, $\hat{\alpha} > 1$;

Decide intruder is moving toward from sensor, $\hat{\alpha} < 1$.

IV. SIMULATION RESULTS

In this section we have simulated a human intruder passing through the FOV of a PIR having $F = 4$ segments and $\gamma = 7.5^\circ$. The intruder moves with a constant speed of $v = 5$ kmph in a straight line making angle with the main PIR sensor axis of $\psi = 50^\circ$ away from the sensor. The intruder's temperature is $T_i = 37^\circ$ with emissivity $\varepsilon = 1$, environment temperature $T_e = 20^\circ$, sensor area $A_s = 20 \mu\text{m}^2$ and intruder area $A_i = 0.7 \text{m}^2$. The PIR sensor has $K = 6. \times 10^3$, $\tau_t = 4.2$ sec, and $\tau_e = 1$ sec. The noise in the system is zero-mean AWGN with standard deviation of $50 \mu\text{V}$.

We compare the detection performance via ROC graphs showing the probability of detection (P_D) against the probability of false alarm (P_{FA}) of the ED in (10), the EWD in (21), and the PD in (23) (both use $L = 3$ sinusoidal components) in a Monte Carlo simulation with 10^5 iterations. Two sets of simulations are run, one with the intruder moving away from the sensor and the second when the intruder is moving toward the sensor. Figs. 4-8 depict the ROC for different R_0 values when the intruder is moving away from the sensor, whereas Figs. 9-13 show the ROC when the intruder is moving toward the sensor. In general, for a relatively small distance, both the EWP and the PD achieve a similar performance as shown in Figs. 4, 5, 9, and 10, while still performing better than the ED. On the other hand, the rest of the figures show the superior performance of the EWD over large distances. Finally, the direction of movement is estimated by the EWD algorithm, by testing the $\hat{\alpha}$ as mentioned before. The EWD achieves almost 100% correct direction estimation for all different distances as shown in Table I.

TABLE I: Direction Estimation

R_0	10m	30m	50m	70m	90m
Intruder moving away	100%	100%	100%	100%	100%
Intruder moving toward	100%	100%	100%	100%	99.89%

V. CONCLUSIONS AND FUTURE WORK

We have investigated the problem of long range intrusion detection using PIR sensors. An inverse square-law relation is established for the incident heat flux and the separation distance. Then, the PIR sensor output signal is modeled by the sum of exponentially modulated sinusoids. Accordingly, an exponentially windowed periodogram detector is proposed showing very good detection performance for long distance cases when compared to both the conventional periodogram detector and the energy detector. In future work, we intend to investigate the use of sensor arrays for intrusion detection.

ACKNOWLEDGMENT

Research presented in this paper was funded by Al-Zaytoonah University of Jordan grant (8/12/2014). The authors gratefully acknowledge this support.

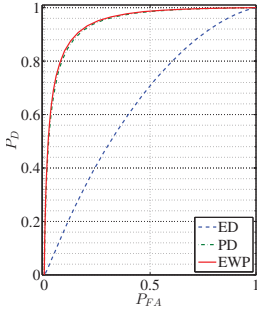


Fig. 4: ROC for $R_0 = 10\text{m}$ and intruder moving away from sensor.

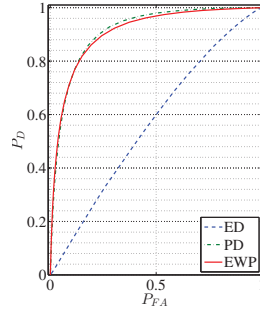


Fig. 5: ROC for $R_0 = 30\text{m}$ and intruder moving away from sensor.

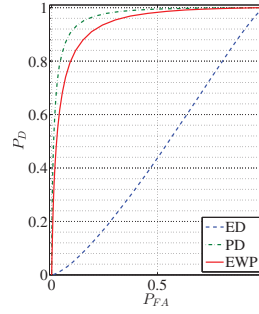


Fig. 9: ROC for $R_0 = 10\text{m}$ and intruder moving toward from sensor.

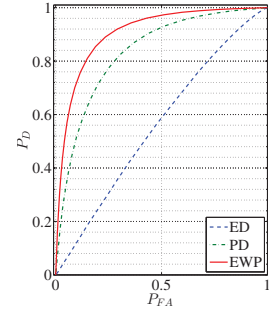


Fig. 10: ROC for $R_0 = 30\text{m}$ and intruder moving toward from sensor.

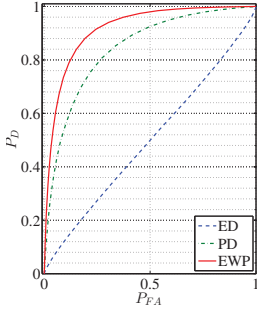


Fig. 6: ROC for $R_0 = 50\text{m}$ and intruder moving away from sensor.

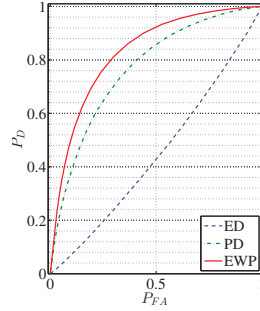


Fig. 7: ROC for $R_0 = 70\text{m}$ and intruder moving away from sensor.

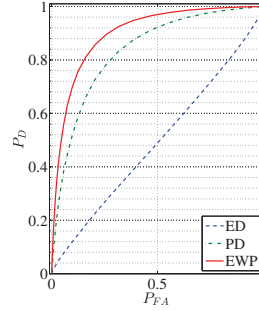


Fig. 11: ROC for $R_0 = 50\text{m}$ and intruder moving toward from sensor.

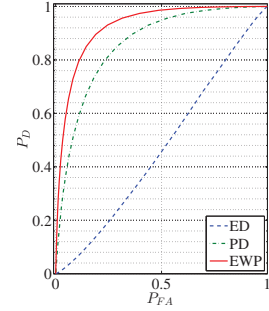


Fig. 12: ROC for $R_0 = 70\text{m}$ and intruder moving toward from sensor.

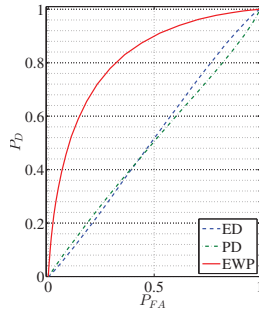


Fig. 8: ROC for $R_0 = 90\text{m}$ and intruder moving away from sensor.

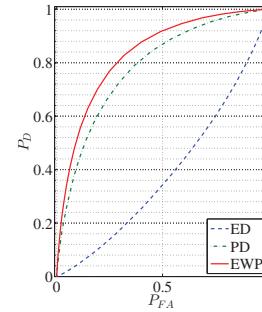


Fig. 13: ROC for $R_0 = 90\text{m}$ and intruder moving toward from sensor.

REFERENCES

- [1] A. Arora, P. Dutta, S. Bapat, V. Kulathumani, H. Zhang, V. Naik, V. Mittal, H. Cao, M. Demirbas, M. Gouda *et al.*, "A line in the sand: a wireless sensor network for target detection, classification, and tracking," *Computer Networks*, vol. 46, no. 5, pp. 605–634, 2004.
- [2] H. Budzier, *Thermal infrared sensors theory, optimization, and practice*. Chichester, West Sussex, U.K. Hoboken, N.J.: Wiley, 2011.
- [3] R.-S. Hsiao, D.-B. Lin, H.-P. Lin, S.-C. Cheng, and C.-H. Chung, "Indoor target detection and localization in pyroelectric infrared sensor networks," *IEEE VTS APWCS. Singapore City: IEEE*, pp. 115–119, 2011.
- [4] S. Akbas, M. A. Efe, and S. Ozdemir, "Performance evaluation of pir sensor deployment in critical area surveillance networks," in *Distributed Computing in Sensor Systems (DCOSS), 2014 IEEE International Conference on*. IEEE, 2014, pp. 327–332.
- [5] L. Gu, D. Jia, P. Vicaire, T. Yan, L. Luo, A. Tirumala, Q. Cao, T. He, J. A. Stankovic, T. Abdelzaker *et al.*, "Lightweight detection and classification for wireless sensor networks in realistic environments," in *Proceedings of the 3rd international conference on Embedded networked sensor systems*. ACM, 2005, pp. 205–217.
- [6] R. Abu Sajana, R. Subramanian, P. V. Kumar, S. Krishnan, B. Amrutur, J. Sebastian, M. Hegde, and S. Anand, "A low-complexity algorithm for intrusion detection in a pir-based wireless sensor network," in *Intelligent Sensors, Sensor Networks and Information Processing (ISSNIP), 2009 5th International Conference on*. IEEE, 2009, pp. 337–342.
- [7] Q. Hao, J.-S. Fang, D. J. Brady, and B. D. Guenther, "Real-time walker recognition using pyroelectric sensors," *IEEE Sensors Journal*, submitted, 2006.
- [8] P. Zappi, E. Farella, and L. Benini, "Tracking motion direction and distance with pyroelectric ir sensors," *Sensors Journal, IEEE*, vol. 10, no. 9, pp. 1486–1494, 2010.
- [9] J. Yun and M.-H. Song, "Detecting direction of movement using pyroelectric infrared sensors," *Sensors Journal, IEEE*, vol. 14, no. 5, pp. 1482–1489, 2014.
- [10] A. Odon, "Modelling and simulation of the pyroelectric detector using matlab/simulink," *Measurement Science Review*, vol. 10, no. 6, pp. 195–199, 2010.
- [11] S. M. Kay, *Fundamentals of Statistical Signal Processing, Volume 2: Detection Theory*. Prentice Hall, 1998.